SUPPLEMENTAL FIGURE LEGENDS

Figure S1. MED1^{IDR} condensates partition a specific functional class of proteins distinct from those partitioned by NPM1, related to Figure 1.

A) Gene ontology analysis of top 40 MED1^{IDR} pellet-enriched (pellet/sup) proteins from proteomics analysis.
B) Heatmap of log_2 fold change values (pellet/sup) from proteomics analysis of two independent fractionation experiments.
C) Venn diagram of top 200 pellet-enriched proteins for MED1^{IDR} and for NPM1.
D) Heatmap representing the presence and absence of indicated proteins.

Figure S2. Genes associated with high local concentrations of MED1 also exhibit the highest transcriptional activity, related to Figure 2.

A) Boxplots (10-90%) representing the read densities (RPKM) for RPB1, CTR9, SPT6, and NELFA at genes associated with enhancer regions with high MED1 occupancy (super-enhancers, SE, orange) or with low MED1 occupancy (typical enhancer genes, TE, grey) in mouse embryonic stem cells.
B) Metagene plot of RNA Pol II S5 phosphorylation (S5ph) read densities (RPM, reads per million) at gene body (TSS-TES) +/- 2-kb for genes proximal to annotated enhancers in mESCs that either have high MED1 occupancy (super-enhancers, SE, orange) or low MED1 occupancy (typical enhancers, TE, gray).
C) Same as S2B, but for RNA Pol II S2 phosphorylation (S2ph).
D) Highest occupancy of MED1 at a gene's enhancer correlates with highest occupancy of S5 and S2 phosphorylated RNA Pol II within the gene body.
E) Highest occupancy of MED1 at a gene's enhancer correlates with lowest traveling ratio of RNA Pol II.
F) Representative images of IF for MED14 (magenta) at indicated CFP-LacI control or MED1 fusion. Scale, 5μm.
G) MED1^{IDR} does not partition the Mediator complex. IF quantification of MED14 from experiments in S2F at indicated CFP-LacI control or MED1 fusion. Mean±SEM. p-values, one-way ANOVA vs CFP-LacI.

Figure S3. MED1^{IDR} is required for gene activation during a cell-state transition, related to Figure 3.

A) Immunofluorescence in 3T3-L1 cells for MED1 (top row) and CTR9 (left middle row) or RPB1 (right middle row) before (D0) and three days after differentiation (D3). Scale, 5 μm.
B) Manders overlap coefficient per cell from samples shown in S3A giving a relative score for the degree of co-occurrence between MED1 and CTR9 (left) or RPB1 (right) for undifferentiated (black) or differentiated (pink) cells. Mean±SEM. p-values, two-tailed unpaired t-test.
C) Immunoblot for indicated transcriptional regulators in undifferentiated (D0) and 3-day differentiated (D3) 3T3-L1 cells. Beta tubulin was included as a loading control.
D) Expression of MED1 and other transcriptional regulators is mostly unchanged during 3T3-L1 adipogenesis. Heatmaps representing log_2 fold change in RNA levels.
E) Expression of adipocyte genes occurs in at least two discrete waves. Heatmaps representing log_2 fold change in RNA levels.
F) Relative expression levels from RT-qPCR of siRNA-mediated knockdown targets 3 days after differentiation.
G) Quantification of percentage of cells in field of view with BODIPY (n=5). Mean±SD. p-values, one-way ANOVA vs siRNA control.
H) Schematic of *Med1* gene architecture indicating the exons targeted in 3T3-L1 CRISPR lines.
I) $MED1^{\Delta IDR}$ interacts with Mediator complex. Immunoblot after co-IP of MED1 and MED4.
J) Quantification of percentage of cells in field of view with BODIPY (n=5). Mean±SD.
K) Relative expression levels of genes expressed in the first transcriptional wave of adipogenesis (n=3). Mean±SD. p-values, one-way ANOVA vs NT control.
L) Relative expression levels of adipocyte genes across 7 days of differentiation (n=3). Mean±SD. p-values, one-way ANOVA vs NT control.
M) Adipocyte-activated genes with annotated MED1 occupied enhancers were ranked by the fold increase from undifferentiated to day 2 differentiated and binned into 4 equal bins (n=50). Boxplot. p-values, one-way ANOVA vs first bin.
N) Same as M, but expression relative to siRNA control for indicated knockdown is plotted.
O) Adipocyte-activated genes ranked by average (ΔIDR/NT) and binned into four equal bins (n=92). Boxplot. p-values, one-way ANOVA vs first bin.

Figure S4. IDRs of partitioned factors are necessary and sufficient to recapitulate selective partitioning, related to Figure 4.

A) Cartoon depiction of mCherry-IDR proteins and $mEGFP\text{-}MED1^{IDR}$ partitioning experiments, performed without adding exogenous RNA.
B) Representative micrographs of droplets formed upon mixing recombinant $mEGFP\text{-}MED1^{IDR}$ and indicated mCherry fusion. Scale, 2 μm.
C) Boxplot (10-90%) representation of quantification of mCherry signal inside $mEGFP\text{-}MED1^{IDR}$ droplets presented as condensed fraction (mCherry in/out of droplets). p-values, one-way ANOVA vs no IDR control.

D) Cartoon depiction of mCherry-IDR proteins tested in presence of total RNA but in the absence of mEGFP-MED1^{IDR}.
E) mCherry-IDRs do not form droplets on their own under these reaction conditions. Scale, 10 μm.
F) Boxplot (10-90%) representation of condensed fraction of mCherry signal. p-values, one-way ANOVA vs no IDR control.
G) Cartoon depiction of experimental setup.
H) Representative images of mCherry-MED1^{IDR} (top row) tested for partitioning into indicated CFP-LacI-IDR foci (bottom row). Scale, 5 μm.
I) Boxplot (10-90%) showing quantification of partition coefficient for experiments shown in S4H. p-values, one-way ANOVA vs no IDR control.
J) Cartoon depiction of experimental setup.
K) Representative images of mCherry-IDRs (top row) tested for partitioning into CFP-LacI (no fusion) foci (bottom row). Scale, 5 μm.
L) Boxplot (10-90%) showing quantification of partition coefficients for experiments shown in S4K. p-values, one-way ANOVA vs no IDR control.
M) Cartoon depiction of experimental setup
N) Representative images of additional mCherry-IDRs (top row) tested for partitioning into CFP-LacI-MED1^{IDR} foci (bottom row). Scale, 5 μm.
O) Boxplot (10-90%) showing quantification of partition coefficients for experiments shown in S4N. p-values, one-way ANOVA vs no IDR control.

Figure S5. Patterned blocks of acidic and basic residues in IDRs are necessary and sufficient for selective partitioning, related to Figure 5.

A) Comparative analysis shows partitioned IDRs do not have significant differences in fraction of disorder-promoting amino acids compared to other IDR classes tested (All IDRs, 14088; Extract IDRs, 3956; partitioned IDRs, 200; and excluded IDRs, 200). Boxplots (10-90%) representing the comparison of fraction of disorder-promoting amino acids for listed groups. p-values represent one-way ANOVA with multiple comparisons of partitioned IDRs to all others (ns, $p>0.05$).
B) Same as S5A for fraction aromatic.
C) Sama as S5A for Omega aromatic. In this group IDRs without any aromatic residues were excluded. Therefore, the number for each group are: All IDRs, 10192; Extract IDRs, 2799; partitioned IDRs, 154; excluded IDRs, 135.
D) Partitioned IDRs have a compositional bias for certain amino acids (E, D, K, and R) relative to excluded IDRs. Boxplot (10-90%) representing fraction of all 20 amino acids for either partitioned (orange) or excluded (cyan) IDRs. p-values represent Wilcox test with significance cutoff at $p<0.01$ (****, $p<0.0001$; ***, $p<0.001$; **, $p<0.01$).
E) Same as S5A, for fraction acidic.
F) Same as S5A, for fraction basic.
G) Same as S5A, for NCPR.
H) Same as S5A, for kappa.
I) Same as S5A, for SCD.

J) Correlation analysis of partition coefficient and kappa for all IDRs tested in Lac array cells (Fig 4I and S4O). The r^2 value represents a goodness of fit for a linear regression.
K) Same as S5J, for SCD.
L) Left: NCPR plots for $SPT6^{IDR}$, $SPT6^{IDR}$ CS (charge scramble mutant) or $SPT6^{IDR}$ NCS (non-charge scramble mutant #3).
Middle: representative images of $SPT6^{IDR}$, charge scramble and non-charge scramble $SPT6^{IDR}$ (4 μM) partitioning into GFP-$MED1^{IDR}$ (20 μM) droplets formed in presence of RNA (40 ng/uL). Scale 2 μm.
Right: Boxplot (10-90%) representation of condensed fraction of mCherry signal. p-values represent one-way ANOVA with multiple comparisons relative to the $SPT6^{IDR}$ (***, $p<0.001$; ns, $p>0.05$).
M) Heatmap for kappa (k), fraction of charged residues (FCR), disorder-promoting fraction values (predicted using localCIDER algorithm), number of acidic and basic blocks, and the percentage of sequence identity compared to human sequence were plotted for $CTR9^{IDR}$ as defined by MobiDB for indicated organisms. Each value for individual parameters were normalized to the maximum value of the column and scale bar is represented by color intensities ranging from white to red (min to max).
N) Sequence conservation of charge patches across organisms is represented for $CTR9^{IDR}$ sequence (inside black boxes). Middle black line represents the residue length, and the positioning of basic and acidic blocks (10 amino acid window NCPR≥abs(5)) is shown as dark blue bars or dark red bars, respectively. Sequence conservation of these charge blocks across organisms is represented on top of respective blocks using Clustal alignments.
O) Same as S5M for $SPT6^{IDR}$.
P) Same as S5N for $SPT6^{IDR}$.
Q) Gene Ontology of the top 500 blockiest IDRs in the human proteome and top 500 highest charged IDRs that do not contain blocks. All IDRs in Table S4 were used as background (methods).
R) NCPR plots for the disordered region of CTR9 and transcriptional repressors tested in S5S. See Fig 5B for explanation.
S) Representative images of additional mCherry-IDRs (top row) tested for partitioning into CFP-LacI-$MED1^{IDR}$ foci (bottom row). Insets show magnified region at LacO locus (white box). The white color on bottom-row inset shows IDR overlap with $MED1^{IDR}$ signal. Scale, 5 μm.
T) IDRs of tested transcriptional repressors fail to partition into $MED1^{IDR}$.
Quantification of partition coefficients for experiments shown in panel S5S. Data represented as boxplot (10-90%). p-values represent Dunn's test for multiple comparisons relative to no IDR control (****, $p<0.0001$; ns, $p>0.05$).
U) NCPR plots for $CTR9^{IDR}$ and other IDRs reported to phase-separate by interactions among charged residues. See Fig 5B for explanation.
V) Charged IDRs without patterned charge blocks fail to partition into $MED1^{IDR}$. Representative images of mCherry-IDRs (top row) tested for partitioning into CFP-LacI-$MED1^{IDR}$ foci (bottom row). Insets show magnified region at LacO locus

(white box). The white color on bottom-row inset shows IDR overlap with MED1^{IDR} signal. Scale, 5 μm.

W) Quantification of partition coefficient for experiments shown in panel S5V. Data as boxplot (10-90%). p-values represent Dunn's test for multiple comparisons relative to no IDR control (****, p<0.0001; ns, p>0.05).

Figure S6. Introducing IDRs with alternating charge blocks in NELFE leads to NELF complex partitioning and a decrease in gene activation, related to Figure 6.

A) Representative images of NELFE chimeras tested for partitioning into CFP-LacI foci (no IDR fusion). This is a control for experiments shown in Figure 6B. Scale, 1μm.

B) Boxplot (10-90%) showing quantification of partition coefficient for experiments shown in S6A. p-values represent one-way ANOVA against mCherry without IDR (ns, p>0.05) (n=20).

C) Representative images of control experiments for Figure 6H in Lac array cells. Column 1 shows CFP-LacI focus without MCP signal enrichment (row 1). Columns 2-4 show CFP-LacI-MED1^{IDR} foci (row 3) co-transfected with miRFP670-MCP (row 1) and three different conditions: mCherry only, mCherry-CTR9^{IDR}, or mCherry-SPT6^{IDR} (row 2). Far-red MCP signal is present in CFP-LacI-MED1^{IDR} foci despite mCherry-CTR9^{IDR}/SPT6^{IDR} partitioning (columns 3 and 4, row 1). Scale, 1 μm.

D) Graph showing line profile of relative miRFP670-MCP signal centered at CFP foci from experiments in S6C. Data shown as mean ± SEM (n=10).

E) Quantification of relative miRFP670-MCP signal (line profile method as Fig 2M) in LacO foci from experiments in S6C (n=10). Data shown as mean ± SEM. p-values represent one-way ANOVA test for multiple comparisons against CFP-LacI-MED1^{IDR} co-transfected with mCherry (no IDR).

Figure S7. Patterning of local charge density on IDRs is required for selective partitioning, reporter gene activation, and cell-state transition, related to Figure 7.

A) Heatmap for kappa (k), fraction of charged residues (FCR), disorder-promoting fraction values (predicted using localCIDER algorithm), number of acidic and basic blocks, and the percentage of sequence identity compared to human sequence were plotted for long C-terminal IDRs of MED1 defined by MobiDB for indicated organisms. Each value for individual parameters were normalized to the maximum value of the column and scale bar is represented by color intensities ranging from white to red (min to max).

B) Sliding net charge (10-residue window, black) is shown for long C-terminal IDRs of MED1 defined by MobiDB for indicated organisms. Red bars represent acidic residues and blue bars represent basic residues. Y-axis represents sliding charge index. The positioning of basic patches (10 amino acid window NCPR≥abs (5)) is shown as dark blue bars on top of the boxes. Sequence conservation of these charge patches across organisms is represented on top of respective patches using Clustal alignments.

C) Representative images of mCherry-HP1α^{IDR} tested for partitioning into wildtype and mutant CFP-LacI-MED1^{IDR} foci (listed on left of each row) in Lac array cells. Scale, 1μm.
D) Boxplot (10-90%) of partition coefficient (Z-scores) for mCherry-HP1α^{IDR} relative to the partitioning of mCherry without IDR in wildtype and mutant CFP-LacI-MED1^{IDR} foci. p-values represent one-way ANOVA test for multiple comparisons against HP1α^{IDR} with wildtype MED1^{IDR}, n=10 (***, p<0.001; **, p<0.01).
E) Representative images of mCherry without IDR fusion tested for partitioning into wildtype and mutant CFP-LacI-MED1^{IDR} foci (listed on left of each row) in Lac array cells. These experiments were used as a reference for the Z-score calculation in Figure 7 and S7D. Scale, 1μm.
F) Graph showing line profile of relative mCherry-MCP signal centered at CFP foci from experiments in Figure 7F-7G. Data shown as mean ± SD. n=10.
G) Relative expression levels of *Med1* for indicated addbacks in 3T3-L1 *Med1* KO clones #2 and #15 after 3 days of differentiation. Data are represented as mean ± SD. Values are normalized to the wildtype *Med1* addback. P-values represent one-way ANOVA with multiple comparisons to WT (****, p<0.0001; ***, p<0.001; **, p<0.01; *, p<0.05).
H) Related to Figure 7I. Relative expression of adipocyte genes after induction (day 3) for the indicated addback experiments (x-axis) in *Med1* KO clone #15. Data as mean ± SD. Values are normalized to the positive control (WT). p-values represent one-way ANOVA with multiple comparisons to WT (****, p<0.0001; ns, p>0.05).
I) Representative image of BODIPY staining for NC for *Med1* KO clone #15. Scale, 20μm.
J) Relative expression levels of adipocyte genes in 3T3-L1 *Med1* KO clone #2 + addback experiments after 3 days of differentiation. Data are represented as mean ± SD. Values are normalized to WT. p-values represent one-way ANOVA with multiple comparisons to WT. Related to Figure 7I.
K) Representative images of *Med1* KO clone #2 + indicated addback construct stained after 9 days of differentiation to identify neutral lipid droplet accumulation (BODIPY shown in red) and to identify cell nuclei (DAPI). Scale, 20μm.
L) Quantification of percentage of cells in field of view with BODIPY-stained fat droplets for 3T3-L1 *Med1* KO clone #2 transduced with indicated construct, normalized to wildtype *Med1* (WT), after 9-days differentiation. Data are represented as mean ± SD. n=5 fields of view. p-values represent one-way ANOVA with multiple comparisons to WT (****, p<0.0001).
M) NCPR plots for controls and blocky IDRs listed on the left and tested in Figure 7M, S7N.
N) Representative images of “blocky IDRs” (listed on top) as CFP-LacI fusions tested with different mCherry fusions to assess partitioning (row 1 mCherry without fusion, row 2 for NELFE^{tentacle}, row 3 NELFE$^{blocky\ tentacle}$). White color in merged CFP channel (bottom inset in each row) shows overlap. Scale, 1μm.
O) Boxplot (10-90%) of partition coefficients (Z-scores) showing standardized values relative to no IDR mCherry control for each individual CFP-LacI fusion shown in

S7N (n=20). p-values represent one-way ANOVA test for multiple comparisons against CFP-LacI with no IDR (****, $p<0.0001$; *, $p<0.05$; ns, $p>0.05$).

P) Graph showing line profile of relative mCherry-MCP signal centered at CFP foci from experiments in Figure 7M (row 3). Data shown as mean ± SD (n=10).

Q) Relative expression levels of MED1 chimeras in 3T3-L1 addback experiments normalized to $MED1^{IDR}$ (n=3). Data shown as mean ± SD.

Supplemental Figure 1

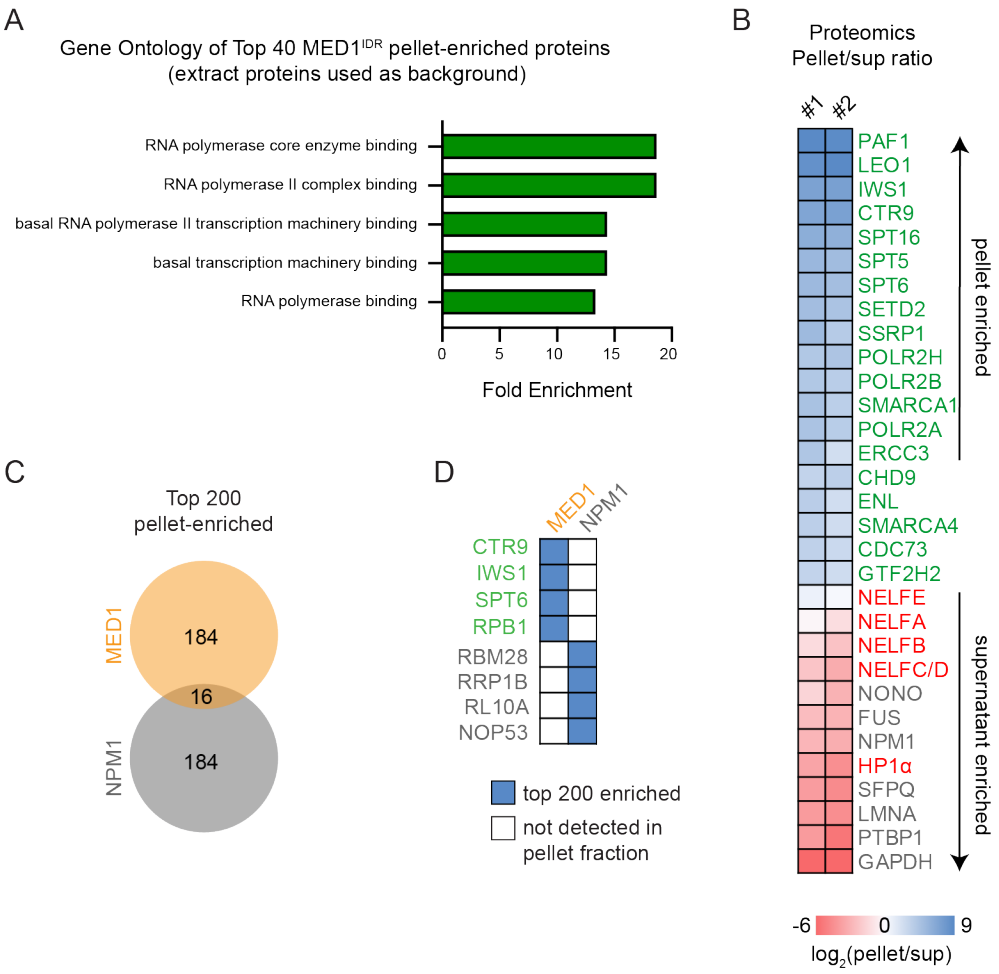

Supplemental Figure 2

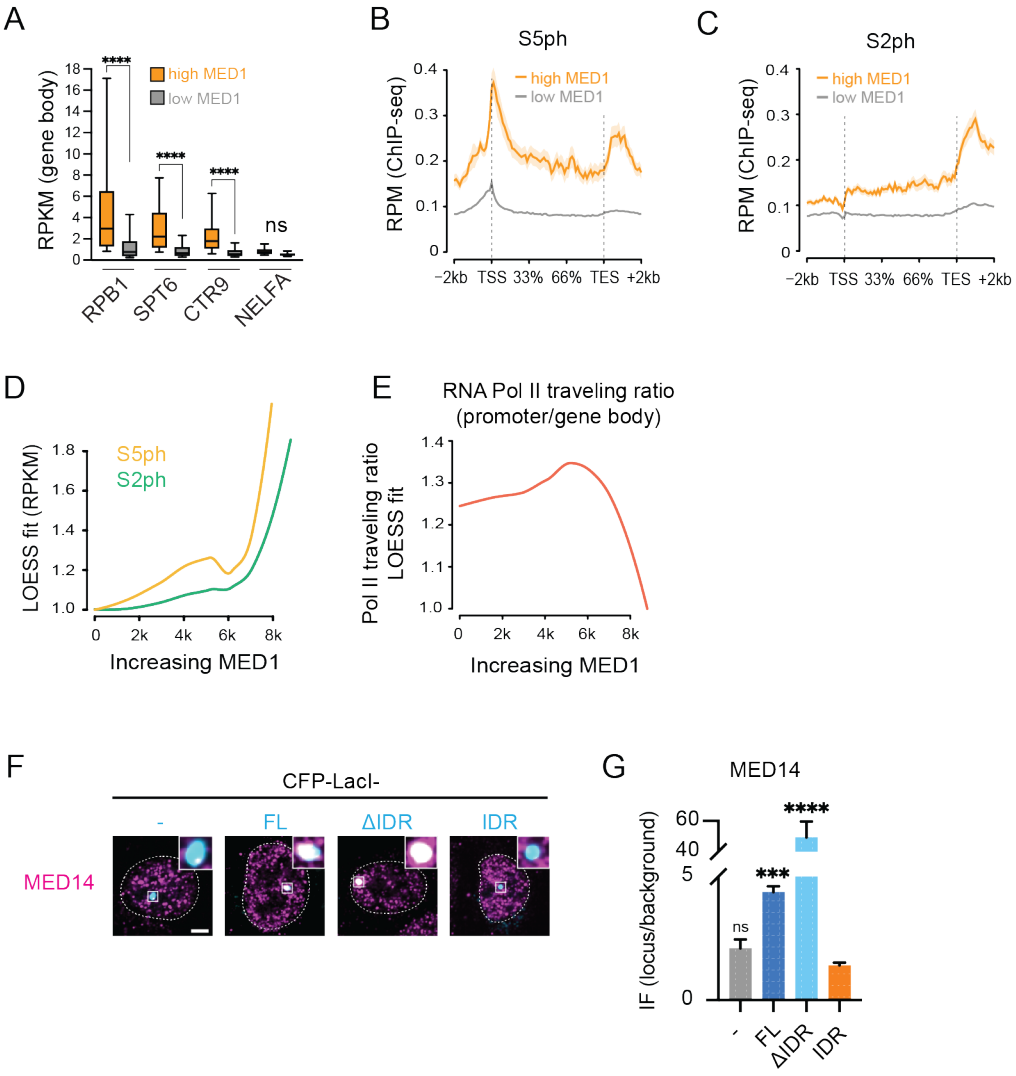

Supplemental figure 3

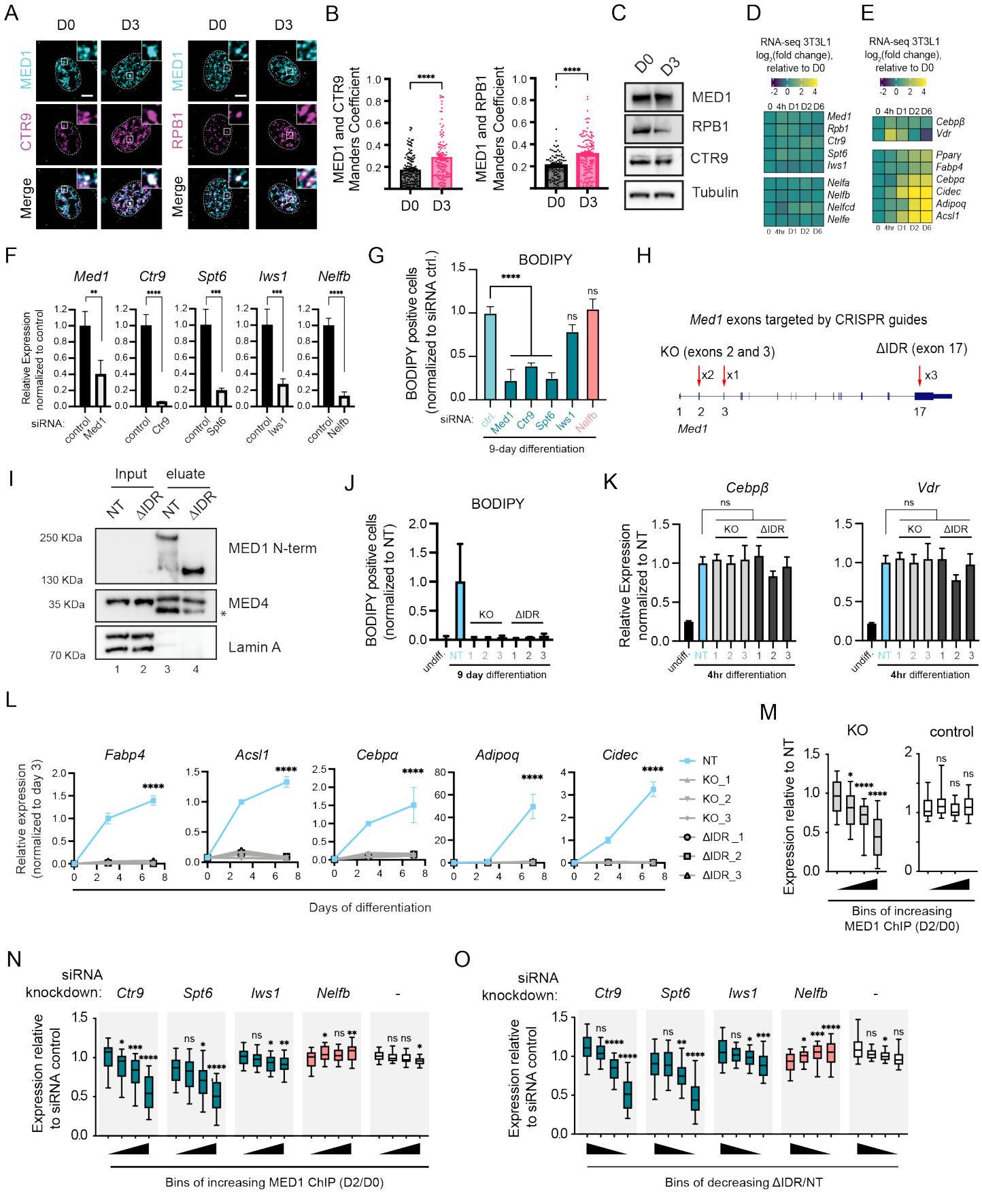

Supplemental figure 4

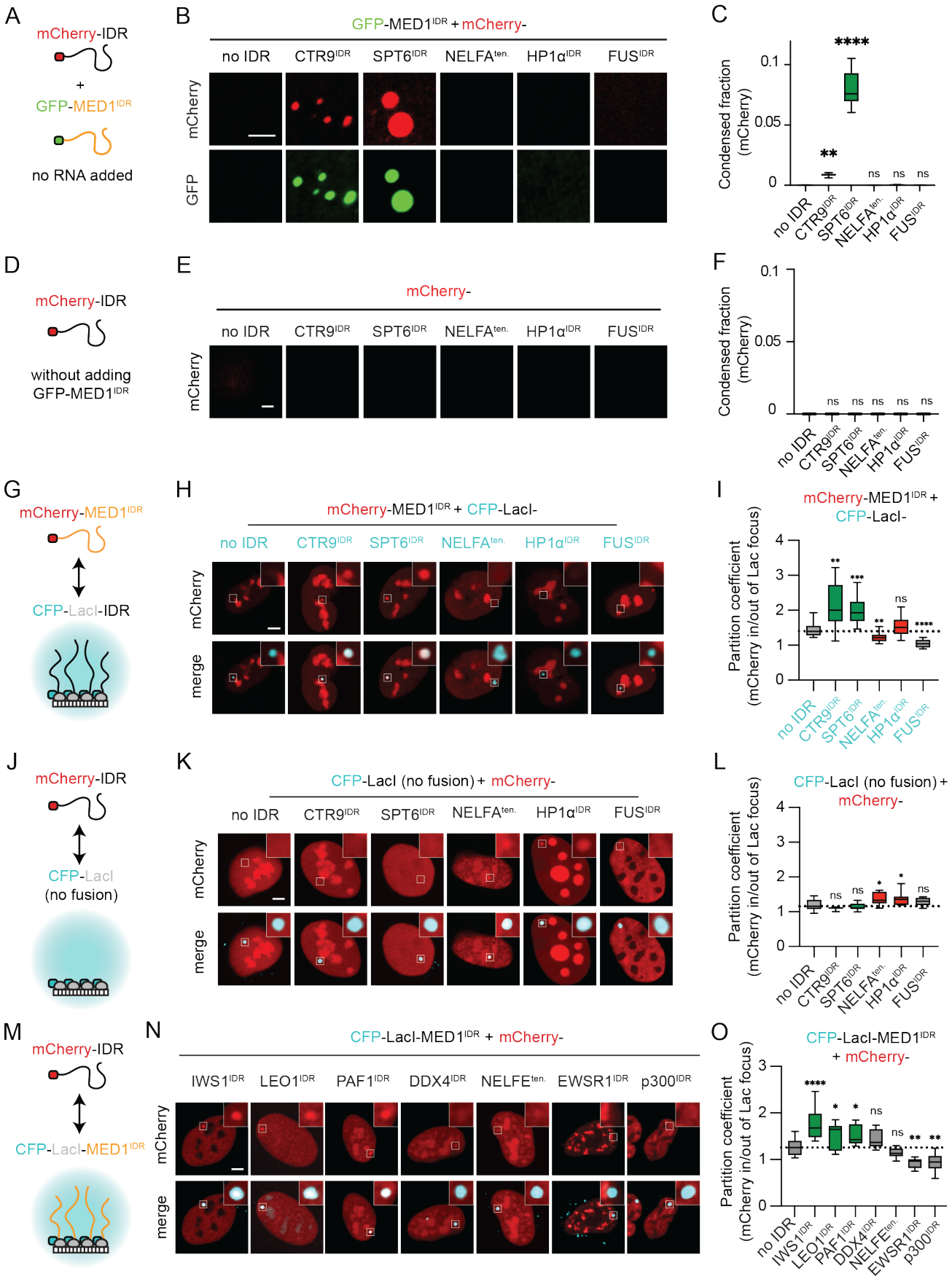

Supplemental figure 5

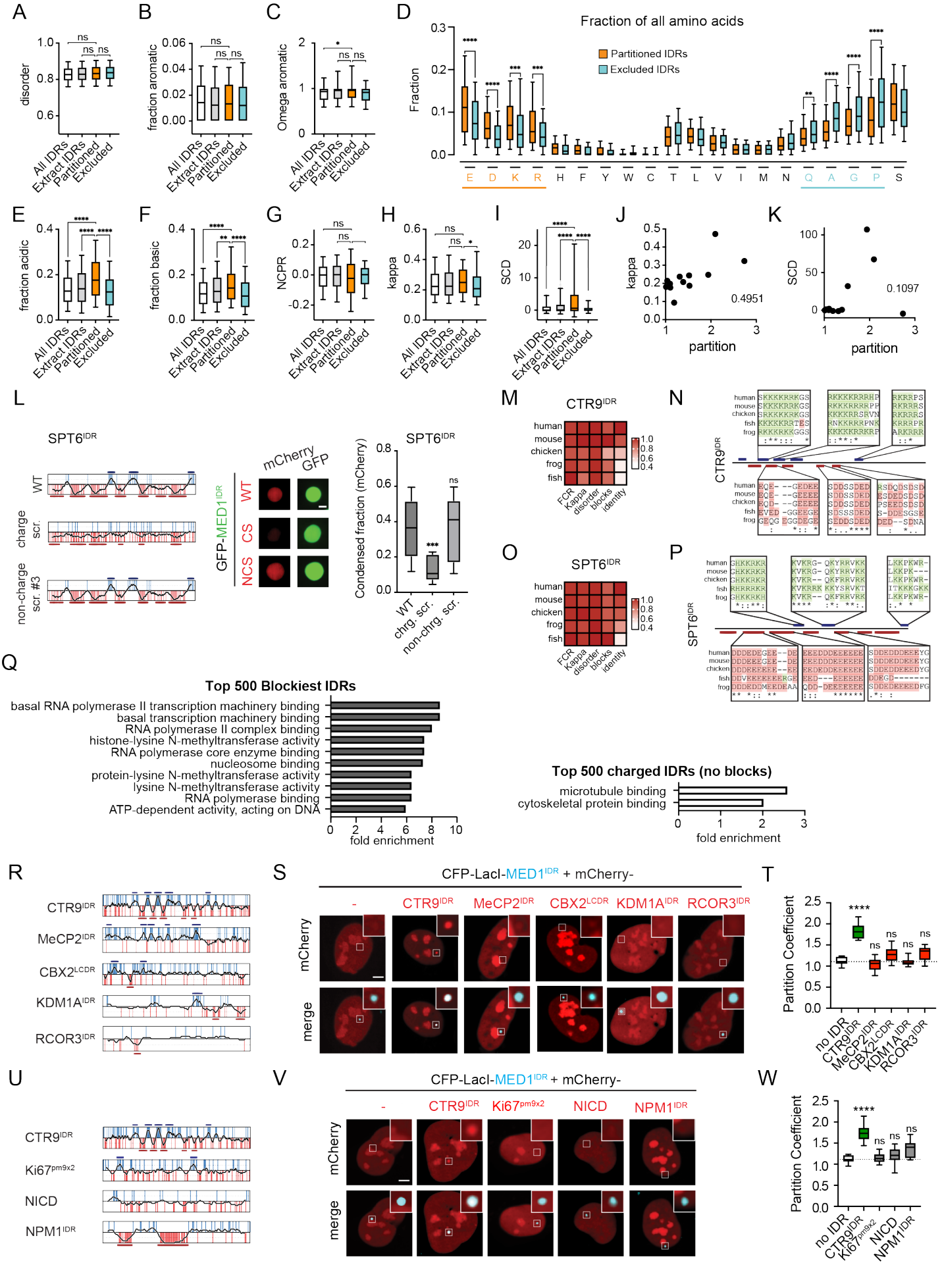

Supplemental figure 6

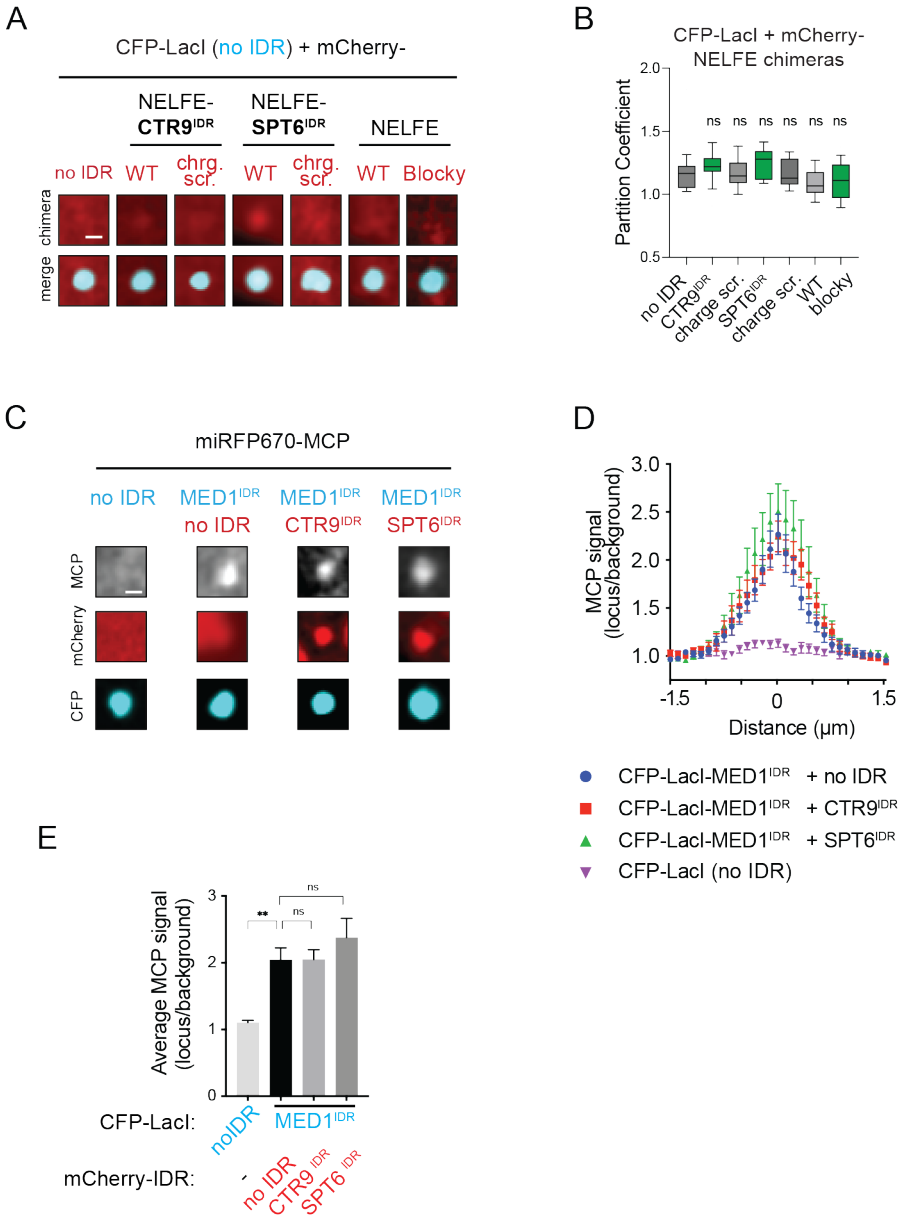

Supplemental Figure 7